Journal of Low Temperature Physics (2025) 219:157–171
https://doi.org/10.1007/s10909-025-03288-1

Influence of Fe/Mo Stoichiometry on Structural and Magnetic Properties in $Sr_2Fe_xMo_{2-x}O_6$: A Theoretical and Experimental Study

Naman A. Naushahi[1,2] · I. Angervo[1] · H. Huhtinen[1] · M. Lastusaari[3] · M. Chromy[4] · A. Ernst[4,5] · P. Paturi[1]

Received: 20 December 2024 / Accepted: 3 March 2025 / Published online: 2 April 2025

Abstract

The influence of nonstoichiometry on the structural and magnetic properties of Sr_2FeMoO_6 (SFMO) has been investigated by varying the ratio of Fe in polycrystalline samples. We demonstrate that changes in the Fe/Mo ratio can elevate the Curie temperature (T_C) in SFMO, even though the total magnetic moment is reduced at the same time. The discoveries of the stoichiometric imbalance between the cations Fe and Mo are discussed in the context of first-principles calculations on the electronic and magnetic structures of SFMO using the GGA+U method. Our theoretical results reveal that Fe deficiency reduces the T_C due to the antiparallel alignment of Fe moments in Mo positions, which is consistent with experimental observations. In contrast, accurate T_C trends for Fe excess are reproduced only by considering spin disorder, with both parallel and antiparallel Fe moment orientations. These insights provide a detailed understanding of the magnetic interactions in SFMO. Our findings lay the groundwork for developing innovative SFMO-based materials and emphasize the significance of stoichiometry control in optimizing SFMO properties.

Keywords SFMO · Nonstoichiometry · Magnetic properties · Curie temperature

✉ Naman A. Naushahi
naman.a.naushahi@utu.fi

[1] Wihuri Physical Laboratory, Department of Physics and Astronomy, University of Turku, FI-20014 Turku, Finland

[2] University of Turku Graduate School (UTUGS), University of Turku, Turku, Finland

[3] Department of Chemistry, University of Turku, FI-20014 Turku, Finland

[4] Institute for Theoretical Physics, Johannes Kepler University, Altenbergerstr. 69, 4040 Linz, Austria

[5] Max-Planck-Institut für Mikrostrukturphysik, Weinberg 2, 06120 Halle (Saale), Germany

1 Introduction

In recent decades, magnetic double perovskites, represented by the general formula $A_2BB'O_6$ (where A stands for alkaline-earth-metal or rare earth-metal cations, and B, B' denote transition metal cations), have garnered significant attention [1–4]. Among these, double perovskite Sr_2FeMoO_6 (SFMO) has gained extensive study due to its high Curie temperature ($T_C \approx 420$ K) and half-metallic behavior, providing complete (100%) spin polarization [5]. These characteristics are important for spintronics applications, including magnetic tunnel junctions and spin injectors [6]. Thus, it seems that SFMO is a good fit for incorporation into spin electronic devices. However, it has been discovered that the manufacturing factors of this compound are extremely sensitive and significantly impact its structural defects and, consequently, its magnetic and transport properties [7–13]. Also, the magnetotransport properties of SFMO and other double perovskites can be adversely affected by defects such as anti-site disorder (ASD) and nonstoichiometry [14–16].

In a perfectly ordered SFMO, Fe and Mo cations are arranged in NaCl-like pattern, separated by oxygen anions, and their magnetic moments are antiferromagnetically coupled [5].

However, a certain amount of disorder is fundamentally introduced during the synthesis of SFMO, whether it is done in bulk sintered form, single-crystalline structure, or epitaxial thin-film growth. Potential defects encompass nonstoichiometry arising from excess Fe or Mo, ASD due to simultaneous replacement of Fe with Mo and vice versa, the presence of oxygen vacancies (V_O), and the development of extended phases. It has been found that M_s and T_C values are associated with the composition x in $Sr_2Fe_{1+x}Mo_{1-x}O_6$; magnetization is affected by V_O concentration, whereas cation ordering determines M_s values and spin polarization [17–20]. In previous work [17], the elevation of T_C in $Sr_2Fe_{1+x}Mo_{1-x}O_6$ with $x > 0$ was explained by kinetic energy gains arising from increased spin polarization among itinerant electrons within the ferromagnetic Fe background. This effect is driven by the augmented concentration of Fe and a reduced Fe-Fe separation. The substitution of Mo with Fe beyond $x = 0$ results in a structured Fe-O-Fe-O-Fe sequence, enhancing the ferromagnetic coupling between Fe ions on the same sub-lattice and leading to an incremental T_C, especially in the presence of minimal mis-site disorder.

Kobayashi et al. [21] and Sugata et al. [22] investigated $Sr_2Fe(W_{1-x}Mo_x)O_6$ by introducing W at the Mo site. They observed a ground state transition from an antiferromagnetic insulator to a ferromagnetic metal. In a similar context, Yuan et al. [23] explored $Sr_2(Fe_{1-x}Cu_x)MoO_6$, introducing Cu at the Fe site. Their study revealed that a higher degree of Fe/Mo ordering was observed with heavy Cu doping at the Fe site, leading to a transition from semiconductor to metal. G.Y. Liu et al. [24–26] examined the structural, magnetic, and transport properties of $Sr_2Fe_xMo_{2-x}O_6$ and related these properties with the degree of Fe/Mo ordering. A few attempts have been made to examine the effect of strontium nonstoichiometry and various oxygen concentrations ($O_{6-\delta}$) in SFMO [8, 27–29]. There have been

studies conducted on sintered SFMO found that the Fe and Mo ions deviate from their respective sub-lattices [1, 14, 30]. Extensive research has been conducted on site doping with Mo or Fe but there is a notable gap in studies focusing on the alteration of the Fe/Mo ratio.

According to both theoretical and experimental data, the magnetic properties of SFMO are largely dependent on the configuration of oxygen vacancies, ASD, and stoichiometric imbalance [5, 31–33]. The occurrence of oxygen vacancies and ASD, which is defined by the incorrect positioning of Fe in Mo sites and vice versa, usually lowers saturation magnetization (M_s). The lower M_s of 3 μ_B/f.u. at 4.2 K in SFMO, which is associated with the ASD, serves as an example of this [5]. Some degree of ASD is currently deemed unavoidable, even in stoichiometric bulk samples [14]. Figure 1 illustrates the schematic representation of excess of Fe and ASD.

The motivation for the present work is rooted in our previous study [34], where we explored the impact of deposition distance on SFMO thin films grown by pulsed laser deposition. The optimal properties were observed at longer distances, including an onset Curie temperature of approximately 400 K. These improvements were attributed to a stoichiometric imbalance between Fe and Mo cations, altering magnetic interactions and enhancing overall properties.

In this study, we explored the effects of Fe/Mo stoichiometry imbalance on the structural and magnetic properties of SFMO samples. We synthesized $Sr_2Fe_xMo_{2-x}O_6$ across a broad range of compositions (Fe = 0.8, 0.9, 1, 1.05, 1.1, 1.15, 1.2) and analyzed their structural and magnetic characteristics. To understand the observed magnetic properties, we conducted first-principles calculations using the Green function method within the density functional theory framework. We addressed ASD and excess Fe using a coherent potential approximation and described magnetic properties through Heisenberg exchange constants calculated via the magnetic force theorem. This approach allowed us to present a detailed theoretical perspective on the relationship between Fe/Mo concentration, magnetic ordering, and Curie temperature. Our findings provide explanations for experimental observations and offer guidance for future efforts to optimize SFMO for technological applications. A clear understanding

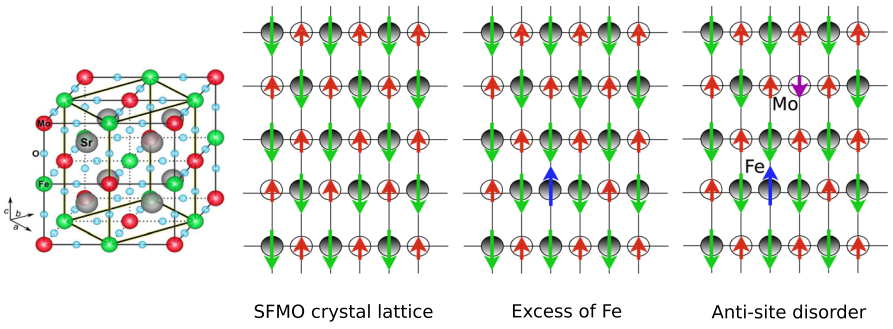

Fig. 1 Schematic illustration of the ASD where simple SFMO crystal (left), the excess of Fe atoms placed on the Mo sites (middle) and Mo atom replaced with Fe atom and vice versa and their stoichiometry imbalance (right). The solid circles represent Fe and open circles represent Mo, while the arrows represent the magnetic moments of the atoms

of nonstoichiometry and its role in modulating the magnetic properties of bulk SFMO is imperative for advancing these applications.

2 Experimental Details

A set of seven polycrystalline SFMO samples were prepared by solid-state reaction method using earlier optimized growth parameters [35, 36]. The synthesis of bulk samples of SFMO frequently employs the solid-state reaction technique which requires high temperatures and long annealing time. Strontium carbonate ($SrCO_3$), iron oxide (Fe_2O_3), and molybdenum oxide (MoO_3) were mixed in nonstoichiometric proportions as part of the preparation for this study. The chemical reaction $4SrCO_3 + Fe_2O_3 + 2MoO_3 + H_2 \rightarrow 2Sr_2FeMoO_6 + 4CO_2 + H_2O$ accounting for the different cation ratios was used to synthesize the nonstoichiometric samples. The nonstoichiometry of the polycrystalline SFMO was managed by changing the MoO_3 and Fe_2O_3 cation ratio.

These raw materials were combined and ground with a mortar and pestle. The powder material was then placed in a pellet press machine to make the powder into a pellet form (10 min at 30 MPa). The solid-state reaction required a tube furnace to heat these pellets to 600°C for 60 h with ramping temperature rates. The initial annealing produced a significant change in the volume and color of the material. At this point, the powders were re-grounded as a part of the solid-state reaction method and pressed again. Then, the pellets were subjected to a high-temperature calcination process at 1100°C for 24 h in flowing Ar+5% H_2+H_2O. The calcination procedure promotes the creation of the SFMO phase in the polycrystalline samples [37].

In order to avoid any structural flaws from arising, the bulk SFMO samples were slowly ramped down to room temperature after calcination.

The crystal structures of the sintered SFMO pellets were investigated by X-ray diffraction (XRD) at room temperature using a Panalytical Empyrean diffractometer with a 5-axes goniometer using CuK_α radiation. The crystallinity, phase purity, and lattice parameters of polycrystalline SFMO were determined from $\theta - 2\theta$ scans within the angular range 10° – 120°. Rietveld refinement was performed by Maud software for polycrystalline SFMO samples [38]. The cation nonstoichiometry was confirmed by X-ray fluorescence spectrometry (XRF) with Panalytical Epsilon 1 spectrometer. The magnetic measurements were done using a Quantum Design MPMS SQUID magnetometer with an external magnetic field. The temperature-dependent field-cooled (FC) magnetizations were measured between 10 K and 500 K in 100 mT field, and the Curie temperature was defined as the minimum of the temperature derivative of the FC curve. To determine the saturation and coercivities, the magnetic hysteresis loops were measured at 10 K between ±1T.

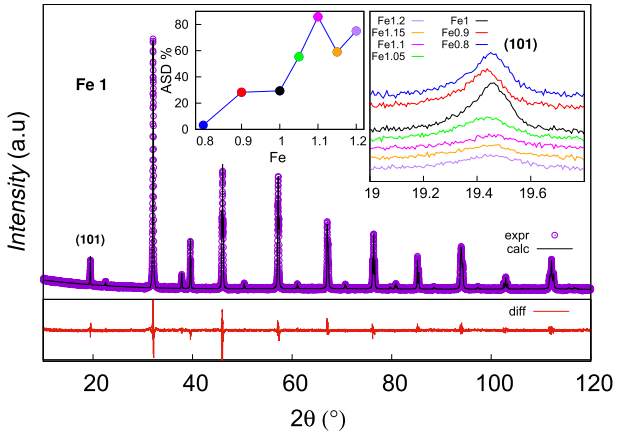

Fig. 2 Rietveld refinements on the XRD data of the sample Fe-1 (main panel). Purple round symbols present the experimental data, the black solid line indicates the simulated XRD profile. The bottom red continuous line stands for the difference between the experimental and theoretical patterns. The right inset shows the evolution of the (00 l) peak around $\theta = 19.4^{\circ}$ for all the samples. The left inset shows the amount of ASD % as a function of increasing amount of Fe

3 Results and Discussion

3.1 Effect of Cation Ratio on Structural Characteristics

The confirmation of cation nonstoichiometry in the SFMO polycrystalline samples was achieved through x-ray fluorescence spectrometry (XRF) which allowed for the precise quantification of the elemental composition within the samples, highlighting any deviations from the expected stoichiometric ratios of strontium, iron, and molybdenum.

The Fe concentration values are as expected and listed in the second to last column of Table 1.

To determine the structural parameters, the experimental XRD data of all the samples were subjected to Rietveld refinement. The refinement was obtained with the Maud XRD analysis program [38]. Only SFMO peaks are detected, and we

Table 1 Values of parameters obtained from the Rietveld refinement using the structural model as well as the refined ASD percentage. The Fe concentration values given in the second last column are measured by XRF

Sample	a (Å)	c (Å)	$\chi 2$	Fe_x (XRF)	ASD(%)
Fe−0.8	5.5704(1)	7.9049(2)	1.424	0.80	3
Fe−0.9	5.5811(1)	7.9072(2)	1.449	0.90	28
Fe-1	5.5708(1)	7.9000(1)	1.342	1	29
Fe−1.05	5.5727(2)	7.9031(3)	1.573	1.04	55
Fe−1.1	5.5736(2)	7.8998(4)	1.531	1.10	85
Fe−1.15	5.5720(2)	7.8980(2)	1.333	1.14	59
Fe−1.2	5.5704(1)	7.8968(2)	1.318	1.19	75

conclude that the SFMO polycrystalline samples are phase pure. The refined XRD pattern together with the Rietveld refinement for Fe-1 sample is displayed in Fig. 2 (main panel), where the black solid line represents the simulated diffractogram, the purple round symbols correspond to the experimental data, and the red line indicates the difference between the experimental and theoretical patterns.

The results from the Rietveld refinement for the a and c parameters are shown in Table 1. The standard deviation of the last numbers are shown in parenthesis, and it is the error of the last digit. The lattice parameters a and c as a function of Fe concentration are also graphically presented in Fig. 3 accompanied by error bars. The performance of Rietveld refinement in this study was assessed based on several fitting parameters, including the chi-square factor (χ^2), profile (Rp), and weighted profile factor (Rwp). All the refinements were satisfactory, as indicated by the (χ^2) values shown in Table 1. The refinement gives lattice parameter values that are quite close to the values reported in the literature, $a = b = 5.575$ Å and $c = 7.893$ Å [39]. As the concentration of Fe increases, there is a subtle variation in the lattice parameter a and a slight decrease is observed in the lattice parameter c.

The observed subtle variations have been attributed to the valencies of Fe^{2+} and Mo^{6+} ions, along with the significantly larger ionic radius of Fe^{2+} (0.78 Å) when compared to Fe^{3+} (0.645 Å) [40]. Also, the increasing concentration of anion vacancies and order among Fe/Mo cations can have an effect [8]. The presence of vacancies and valence disproportion may result in a reduction in the unit cell volume as the Fe content increases [25]. This is concurrent with the observation that the Fe-O(1) bonds shorten and the Mo-O(1) bonds lengthen, demonstrating a compression of the FeO_6 octahedron and an elongation of the MoO_6 octahedron along the SFMO c-axis [8]. There are complex effects arising from factors like the interplay of ionic radii or the presence of defects in samples with different Fe-stoichiometry. Additionally, oxygen vacancies could have an impact on the observed variations in the lattice parameters [29, 33, 41].

The right inset in Fig. 2 shows the evolution of (101) peak intensity reflecting the Fe/Mo ordering [42]. It appears that, with increasing Fe concentrations, the (101) SFMO superstructure peak intensity decreases. This is related to the substitution of Fe for Mo, which destroys the regular arrangements of B-site in the double perovskite structure [43–45].

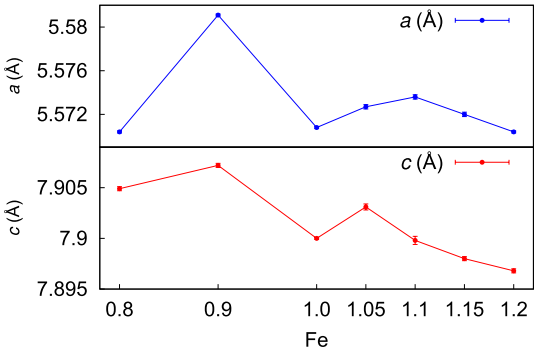

Fig. 3 Graphical representation of a and c parameters with error bars as a function of Fe concentration

This disorder gives rise to the formation of new Fe_{Mo}-O-Fe and Mo_{Fe}-O-Mo bonds [31]. The variation of ASD with sample nonstoichiometry is shown in the top left inset of Fig. 2. The ASD concentration was determined by allowing the occupation of Fe and Mo ions in both sets of positions to vary while keeping the stoichiometry constant in the Rietveld refinement. The ASD concentrations of all samples are 3, 28, 29, 55, 85, 59, and 75% with growing Fe content as presented in Table 1. By confirming the absence of impurities, it becomes clear that the observed deviations in the material's properties are intrinsic and related to cation nonstoichiometry. This provides confidence in the findings and underscores the significance of nonstoichiometry as a fundamental aspect of the material's behavior, distinct from impurity-induced effects.

In a disordered Fe/Mo sub-lattice, the formation energy for a single pair of anti-sites varies depending on the amount of disorder and their specific arrangements [14]. The orientation of the magnetic moment on the Fe_{Mo} anti-site atoms is influenced by their nearest neighbors, with closer anti-site pairs exhibiting lower formation energy, indicating short-range order in a disordered SFMO. This means that ASD is likely to be found as antiphase boundaries or clusters instead of separated defects. Additionally, in Fe-rich conditions, Fe_{Mo} is the preferred defect, and Mo_{Fe} incurs a higher energy penalty. Conversely, in Mo-rich conditions, Mo_{Fe} anti-sites are favored, while Fe_{Mo} anti-sites incur a higher energy penalty [14]. A more favorable mechanism is observed for anti-sites in SFMO than vacancies for addressing nonstoichiometry. However, the formation energy for both Mo and Fe vacancies in Mo-rich SFMO is observed to be lower than the respective defect formation energies in a Fe-rich environment [14]. This correlation aligns with our findings illustrated in Fig. 2, where higher level of ASD is demonstrated in Fe-rich samples. This can be attributed to the tendency for higher ASD in Fe-rich samples, since the absence of vacancies in these samples leads to increased ASD. The energetics of vacancy formation in Mo-rich versus Fe-rich environments thus correlate with the observed variations in ASD levels, as depicted in our XRD data.

3.2 Modified Magnetic Properties by Varying Fe/Mo Ratio

In Fig. 4, the main panel illustrates the normalized FC magnetization curves as a function of temperature for each of the samples under 100 mT magnetic field. The results were normalized by dividing the magnetization values with the FC magnetization values at 10 K. In the FC curves, the slopes at transition change slowly as Fe concentration increases from Fe−0.8 to nominal concentration Fe-1. The ferro-paramagnetic transition appears sharper, and magnetization is preserved better at higher Fe concentration. The inset graph shows the Curie temperature, T_C, as a function of the stoichiometric imbalance between Fe and Mo. The T_C is determined from the first-order derivative of the FC curve. T_C shows an increasing tendency with increasing Fe concentration up to the nominal stoichiometric concentration Fe-1, having the value of 420 K. After that the T_C values remain round 430 K, being clearly higher than the earlier reported around 400–420 K [46, 47].

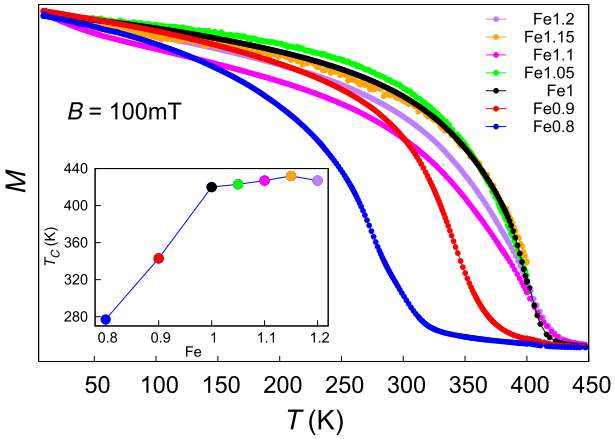

Fig. 4 Normalized field-cooled magnetization as a function of temperature for each sample measured in 100 mT field (main panel). The inset shows the Curie temperature T_C as a function of Fe concentration

It has been observed that sufficiently high ASD concentrations resulting in a strong antiferromagnetic coupling between Fe-O-Fe lead to an increase in T_C [48], as is also seen here. In addition, the theoretical and experimental investigations reported that higher oxygen vacancy concentration could increase T_C. A rise in the number of oxygen vacancies and ASD, attributed to variations in the ferromagnetic (FM) and antiferromagnetic (AFM) magnetic couplings between Fe and Mo ions, results in a notable and robust increase in T_C [33]. The ASD defects facilitate Fe-O-Fe_{Mo} and Mo-O-Mo_{Fe} bonds resulting from a stoichiometric imbalance between Fe and Mo in SFMO [49]. Figure 1 depicts the schematic representation of excess of Fe and ASD, where Fe substitutes on a Mo site with a spin↑ configuration, inducing super-exchange interactions [50]. The reasons for these reported findings will be further discussed in the theoretical model section.

Figure 5 shows partial hysteresis loops of SFMO samples recorded at 10 K. The results were used to determine saturation magnetization M_s and coercivity fields B_c, which are shown in the inset of Fig. 5 as a function of increasing Fe concentration. It was observed that at compositions Fe−0.8, Fe−0.9, and Fe-1, the saturation magnetization has a maximum and diminishes from there on. The diminished magnetization can be ascribed to imperfections such as ASD, oxygen deficiency, and valence disproportion [24, 51]. The reduction in the magnetization is much larger in samples with high concentration Fe samples, which can be attributed to the increased ASD in these samples [52, 53]. The ASD disrupts the collinear alignment of atomic moments between the B and B′ sub-lattices, which is illustrated in Fig. 1. Antiferromagnetic coupling of Fe spins on the Mo site with regular Fe spins can lead to a decrease in M_s [17, 51]. This observation aligns with the previously proposed models [45, 54]. However, an alternative hypothesis suggests that the decline in M_s is primarily due to a reduction in the net magnetic moment of individual Fe sites. Remarkably, this reduction occurs, while the ferromagnetic alignment is maintained [55], signifying that the nearest Fe sites within an ASD continue to couple

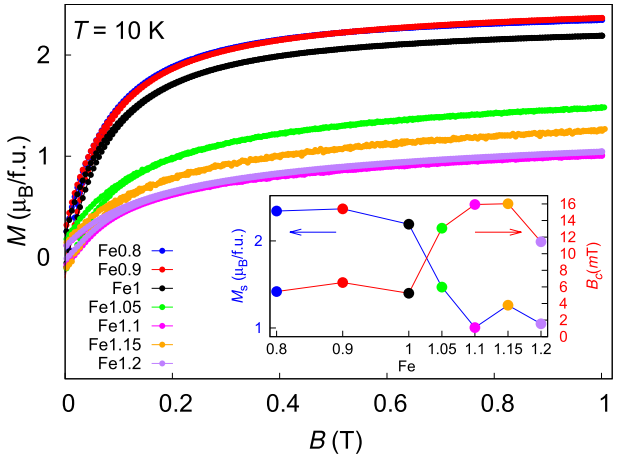

Fig. 5 First quadrants of the hysteresis loops between ±1T measured at 10 K (main panel). The inset shows the saturation magnetization M_s (left side) and coercive field B_c (right side) as a function of Fe stoichiometric imbalance

ferromagnetically. The variation of M_s with Fe/Mo imbalance has been documented in the literature [41, 56, 57]. Additional factors such as valence disproportion and oxygen vacancies are possible causes for the reduction in magnetization. Additionally, it has been observed that high concentrations of ASD can disrupt the spin polarization of charge carriers, further impacting the material's magnetic properties [55, 58].

Our findings indicate that as Fe concentration increases, the B_c values increase. Inset of Fig. 5 (red) illustrates the relationship between B_c and Fe concentration. The observed increment in B_c with higher Fe concentration can be elucidated as the presence of ASD leads to a higher density of antiphase boundaries. Consequently, the magnetic domain walls experience increased pinning, making the process of magnetic domain rotation more challenging under a constant external field [59].

4 Theoretical Model

Previous studies have explored various mechanisms to explain trends in the T_c such as oxygen vacancies, ASD, and point defects in SFMO [14, 17, 28]. Strategic carrier doping has been proposed as a method to achieve higher T_C, compensating for the fewer itinerant electrons resulting from the substitution of Mo with Fe [60]. In addition, the antiferromagnetic coupling between Fe^{3+} and Mo^{5+} ions underlies the ferrimagnetic ordering in SFMO [44, 45]. Furthermore, Fe can exist as 2^+ instead of 3^+, and Mo can have a valence of 6^+ instead of 5^+ [58, 61, 62]. The valence mixing, Fe^{3+}-O-Mo-O-Fe^{2+}, undergoes double exchange with itinerant electrons. Experimental confirmation of valence mixing in SFMO for Fe and Mo has been documented in [63, 64]. However, the existing models have proven either not applicable or inconclusive in explaining these phenomena.

To elucidate the current experimental results and provide a theoretical foundation, we have performed a first-principles study on electronic and magnetic structures of SFMO. The calculations were carried out using a Green function method [65] within the density functional theory in a generalized gradient approximation (GGA) [66]. To describe adequately localized 3*d* Fe, a GGA+U method [67] was utilized using an effective $U_{eff} = U - J$ value of 2 eV. The methods and parameters were already successfully applied to study the electronic and magnetic structure of SFMO [68, 69]. In particular, T_c, estimated using Monte Carlo simulations and assuming a presence of oxygen vacancies, was found to be a very good agreement with experiment [69]. However, in the current study, we do not take into account oxygen vacancies to avoid complexity in physical interpretation. As it was shown in our pervious work [69], oxygen vacancies can significantly lower M_s and increase the T_c in SFMO. ASD and the excess of Fe were treated within a coherent potential approximation as it is implemented within the multiple scattering theory [70]. To describe the magnetic properties of SFMO, Heisenberg exchange constants J_{ij} were calculated within the magnetic force theorem [71]. T_C was estimated within a mean field approximation for the Heisenberg model. Although the mean field approximation is known to overestimate T_C, the trend of T_C as a function of Fe concentration in nonstoichiometric positions should be well reproducible.

In the case of Fe deficiency, we assumed that Fe moments in Mo positions are antiparallel to Fe magnetic moments in stoichiometric positions. In the case of Fe excess, we considered three different scenarios: (i) all magnetic moments of Fe are parallel; (ii) magnetic moments of Fe in nonstoichiometric positions are antiparallel to moments of stoichiometric Fe; (iii) magnetic moments of Fe in nonstoichiometric positions can be parallel and antiparallel to Fe moments in stoichiometric positions with equal probability. Magnetic moments of Mo atoms were considered to be induced, and their orientation depends on the underlying order of Fe moments. In the stoichiometric SFMO, Fe atoms possess a magnetic moment μ=4.12 μ_B, while Mo moments of μ=−0.62 μ_B are antiparallel to Fe moments. The magnetic moments for Fe and Mo in Fe-excess (Fe−1.1) and Fe-deficient (Fe−0.8) configurations were calculated using GGA+U. In the Fe-excess case, the Fe moments at the Fe and Mo sites are 4.05 μ_B, 4.19 μ_B, and −4.44 μ_B, respectively, while the Mo moment is −0.59 μB. For the Fe-deficient configuration (Fe−0.8), the Fe site exhibits a moment of 4.19 μ_B, and the Mo moments are −0.61 μ_B (Mo site) and 0.52 μ_B (Fe site). The results of our simulations are presented in Fig. 6.

Our model for the Fe deficiency reproduces correctly the experimental trend shown in Fig. 4: T_C reduces with the decrease in Fe concentration. This confirms that Fe moments in Mo positions are antiparallel to Fe moments in stoichiometric positions. Mo atoms in Fe stoichiometric positions possess induced magnetic moments of μ=0.52 μ_B, which are parallel to Fe moments in stoichiometric positions. However, the same scenario for the Fe-excess case does not work: T_C decreases with the increase in Fe concentration, which disagrees the experimental results (Fig. 4). Therefore, we have tried two other models for magnetic order in

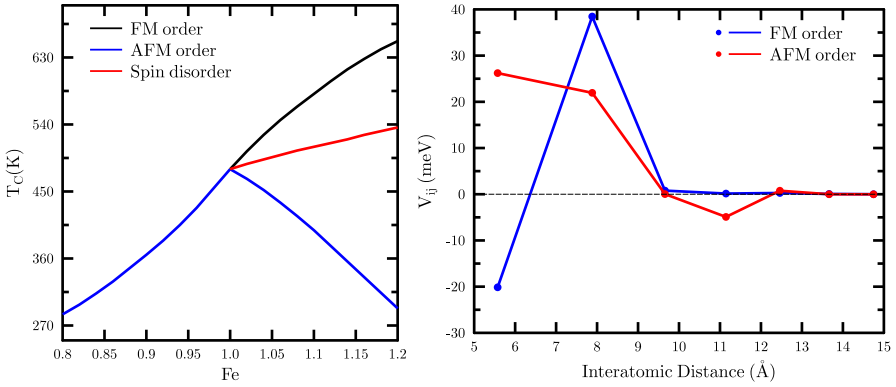

Fig. 6 T_C as a function of Fe concentration calculated for different theoretical models: all Fe moments are ferromagnetic (black line), moments of the excess Fe are antiparallel to the Fe moments in stoichiometric positions (blue line), and moments of the excess Fe are parallel and antiparallel to the Fe moments in stoichiometric positions with the equal probability (red line) (left panel). Mo-Fe effective pair interaction in SFMO for parallel (blue) and antiparallel (red) alignment of Fe magnetic moments (right panel)

this case. First, we assumed that moments of the nonstoichiometric Fe are parallel to moments of the stoichiometric Fe. In this case, T_C increases almost linearly with increase in the nonstoichiometric Fe concentration. Apparently, this behavior also contradicts the experimental trend. Only assuming that moments of the nonstoichiometric Fe can have both parallel and antiparallel orientation of moments (spin disorder), we could reproduce correctly as illustrated by the red line in Fig. 5. Our total energy calculations show that the AFM configuration is only 0.5 meV lower in energy than the FM one assuming a random distribution of the nonstoichiometric Fe atoms. However, Fe atoms can cluster in the sample having the ferromagnetic order 0.3 meV lower in energy than the AFM order. Comparison of our T_C calculations with the experiment shows that both scenarios take place in the same sample.

To describe a possible distribution of nonstoichiometric Fe atoms depending on the magnetic moment orientation in the Fe-excess case, we have calculated the Mo-Fe effective pair interaction using the generalized perturbation method as it is implemented within the multiple scattering theory [72]. The effective pair interaction in a binary alloy with atoms A and B is given by

$$V_{ij} = V_{ij}^{AA} + V_{ij}^{BB} - V_{ij}^{AB} - V_{ij}^{BA}, \tag{1}$$

where i and j index the lattice vectors in real space. $V_{ij} < 0$ corresponds to segregating alloys (phase separation, clustering), while $V_{ij} > 0$ corresponds to ordering alloys. In SFMO for the Fe-excess case (in particular for the concentration of 1.1), nonstoichiometric Fe atoms with moments antiparallel to the moments of stoichiometric Fe atoms tend to an ordered alloy since V_{ij} is positive for the nearest and next nearest neighbors (see right panel of Fig. 5). In the case of the parallel alignment of the Fe moments, the situation is controversial: the nearest neighbors tend to

clustering ($V_{ij} < 0$), while the effective pair interaction with the next nearest neighbors is positive and large showing the tendency to an ordered alloy. We interpret these results as following: Excess Fe atoms, which possess magnetic moments parallel to the moments of the stoichiometric Fe, can surround a Mo atom with the antiparallel ordered moment forming a small cluster around. However, the excess Fe moments can be ordered also antiparallel to the stoichiometric Fe moments (parallel to Mo moments), since the effective pair interaction is comparable to the previous case, however, without clustering. The effective pair interaction energies demonstrate that Fe moments on the Mo site prefer to be parallel to the moment of the stoichiometric Fe in its vicinity and antiparallel otherwise.

5 Conclusions

In this study, we investigated the impact of nonstoichiometry on the magnetic properties of SFMO. Our analysis showed that the T_C increases with higher Fe concentrations, driven by a complex interplay between ferromagnetic (FM) and antiferromagnetic (AFM) couplings, which are significantly influenced by the increased presence of Fe ions. As Fe concentration rises, ASD also increases, affecting the magnetic interactions within the material. Interestingly, the total magnetic moment M_s was observed to decrease with increasing Fe content, explained by variations in the magnetic coupling between Fe and Mo ions, where the balance between FM and AFM interactions shifts. Our theoretical model supports these findings by demonstrating that Fe deficiency leads to a decrease in T_C due to the antiparallel alignment of Fe moments, aligning with experimental trends. Moreover, total energy calculations suggest that for Fe excess, both AFM and FM configurations coexist in the sample due to their comparable energies. Effective pair interaction calculations indicate that excess Fe atoms with antiparallel moments to stoichiometric Fe atoms tend to form ordered alloys, while parallel-aligned Fe moments can form small clusters around Mo atoms. This clustering behavior in an iron-rich environment contributes to the observed increase in T_C and the overall magnetic behavior of SFMO. These findings provide a comprehensive understanding of the magnetic interactions in SFMO, elucidating the complex behavior observed experimentally, and underscore the importance of stoichiometry control in optimizing the magnetic properties of SFMO for advanced material applications.

Acknowledgements The Jenny and Antti Wihuri Foundation is acknowledged for financial support. A.E. acknowledges the funding by the Fonds zur Förderung der Wissenschaftlichen Forschung (FWF) under Grant No. I 5384.

Author contributions N.A.N. conducted the experiments and drafted the main manuscript text. I.A. managed the experimental tools, provided supervision, ensured validation, and contributed to manuscript review. M.L. performed the XRR measurements, while A.E. and M.C. carried out the theoretical calculations. H.H. and P.P. provided overall supervision, reviewed the manuscript, and contributed to editing. All authors reviewed and approved the final manuscript.

Funding Open Access funding provided by University of Turku (including Turku University Central Hospital).

Data Availability No datasets were generated or analysed during the current study.

Declarations

Conflict of interest The authors declare that they have no known competing financial interests or personal relationships that could have appeared to influence the work reported in this paper.

References

1. K.I. Kobayashi, T. Kimura, H. Sawada, K. Terakura, Y. Tokura, Nature **395**, 677 (1998). https://doi.org/10.1038/27167
2. Y. Tomioka, T. Okuda, Y. Okimoto, R. Kumai, K.I. Kobayashi, Y. Tokura, Phys. Rev. B **61**, 422 (2000). https://doi.org/10.1103/physrevb.61.422
3. D. Serrate, J.M.D. Teresa, M.R. Ibarra, J. Condens, Matter Phys. **19**, 023201 (2006). https://doi.org/10.1002/chin.200723213
4. M.K. Chung, P.J. Huang, W.H. Li, C.C. Yang, T.S. Chan, R.S. Liu, S.Y. Wu, J.W. Lynn, Phys. B **385–386**, 418 (2006). https://doi.org/10.1016/j.physb.2006.05.140.
5. Y. Zhang, V. Ji, K.W. Xu, J. Alloys Compd. **648**, 374 (2015). https://doi.org/10.1016/j.jallcom.2015.06.242
6. N. Kumar, P. Misra, R.K. Kotnala, A. Gaur, R.S. Katiyar, J. Phys. D: Appl. Phys. **47**, 065006 (2014). https://doi.org/10.1088/0022-3727/47/6/065006
7. S. Colis, D. Stoeffler, C. Meny, T. Fix, C. Leuvrey, G. Pourroy, A. Dinia, P. Panissod, J. Appl. Phys. **98**, 033905 (2005). https://doi.org/10.1063/1.1997286
8. N. Kalanda, V. Turchenko, D. Karpinsky, S.D.M. Yarmolich, M. Balasoiu, N. Lupu, S. Tyutyunnikov, N.A. Sobolev, Phys. Status Solidi B **256**, 1800278 (2019). https://doi.org/10.1002/pssb.201800278
9. N.A. Kalanda, S.E. Demyanov, A.V. Petrov, D.V. Karpinsky, M.V. Yarmolich, S.K. Oh, S.C. Yu, D.H. Kim, J. Electron. Mater. **45**, 3466 (2016). https://doi.org/10.1007/s11664-016-4478-5
10. N. Kalanda, D. Karpinsky, I. Bobrikov, M. Yarmolich, V. Kuts, L. Huang, C. Hwang, D.H. Kim, J. Mater. Sci. **56**, 11698 (2021). https://doi.org/10.1007/s10853-021-06072-0
11. D. Stoeffler, S. Colis, J. Phys. Cond. Mat. **17**, 6415 (2005). https://doi.org/10.1088/0953-8984/17/41/012
12. D. Stoeffler, Mater. Sci. Eng. **144**, 11 (2007). https://doi.org/10.1016/j.mseb.2007.07.036
13. D. Stoeffler, S. Colis, Mater. Sci. Eng. B **126**, 133 (2006). https://doi.org/10.1016/j.mseb.2005.09.036
14. R. Mishra, O.D. Restrepo, P.M. Woodward, W. Windl, Chem. Mater. **22**, 6092 (2010). https://doi.org/10.1002/chin.201102001
15. J. Rager, M. Zipperle, A. Sharma, J.L. MacManus-Driscoll, J. Am. Ceram. Soc. **87**, 1330 (2004). https://doi.org/10.1111/j.1151-2916.2004.tb07730.x
16. S. Sharma, A. Berenov, J. Rager, W. Branford, Y. Bugoslavsky, L.F. Cohen, J.L. MacManus-Driscoll, Appl. Phys. Lett. **83**, 2384 (2003). https://doi.org/10.1063/1.1613358

17. D. Topwal, D.D. Sarma, H. Kato, Y. Tokura, M. Avignon, Phys. Rev. B **73**, 094419 (2006). https://doi.org/10.1103/physrevb.73.094419
18. A.A. Markov, O. Savinskaya, M. Patrakeev, A. Nemudry, I. Leonidov, Y. Pavlyukhin, A. Ishchenko, V. Kozhevnikov, J. Solid State Chem. **182**, 799 (2009). https://doi.org/10.1016/j.jssc.2008.12.026
19. T.S. Chan, R. Liu, S. Hu, J. Lin, Mater. Chem. Phys. **93**, 314 (2005). https://doi.org/10.1016/j.matchemphys.2005.03.060
20. N.M. Ferreira, A. Kovalevsky, E. Naumovich, A. Yaremchenko, K. Zakharchuk, F. Costa, J. Frade, J. Eur. Ceram. Soc. **34**, 2339 (2014). https://doi.org/10.1016/j.jeurceramsoc.2014.02.016
21. T. Kobayashi, K. Nomura, F. Uchikawa, T. Masumi, Y. Uehara, Jpn. J. Appl. Phys. **27**, 1880 (1988). https://doi.org/10.1143/jjap.27.l1880
22. S. Ray, J. Phys.: Condens. Matter **13**, 607 (2001). https://doi.org/10.1016/j.mseb.2005.09.017
23. C.L. Yuan, J. Appl. Phys. **91**, 4421 (2002). https://doi.org/10.1063/1.1454207
24. G. Liu, G. Rao, X. Feng, H. Yang, Z. Ouyang, W. Liu, J. Liang, J. Phys. Cond. Mat. **15**, 2053 (2003). https://doi.org/10.1002/chin.200324010
25. G. Liu, G. Rao, X. Feng, H. Yang, Z. Ouyang, W. Liu, J. Liang, J. Alloys Compd. **353**, 42 (2003). https://doi.org/10.1002/chin.200324010
26. G.Y. Liu, Phys. B Condensed Matter **334**, 229 (2003). https://doi.org/10.1016/s0921-4526(03)00070-x
27. L. Harnagea, P. Berthet, J. Solid State Chem. **222**, 115 (2015). https://doi.org/10.1016/j.jssc.2014.11.017
28. M. Saloaro, M. Hoffmann, W.A. Adeagbo, S. Granroth, H. Deniz, H. Palonen, H. Huhtinen, S. Majumdar, P. Laukkanen, W. Hergert, A. Ernst, P. Paturi, A.C.S. Appl, Mater. Interfaces **8**, 20440 (2016). https://doi.org/10.1021/acsami.6b04132
29. M. Saloaro, M.O. Liedke, I. Angervo, M. Butterling, E. Hirschmann, A. Wagner, H. Huhtinen, P. Paturi, J. Magn. Magn. Mater. **540**, 168454 (2021). https://doi.org/10.1016/j.jmmm.2021.168454
30. R. Kircheisen, J. Töpfer, J. Solid State Chem. **185**, 76 (2012). https://doi.org/10.1016/j.jssc.2011.10.043
31. A.B. Muñoz-García, M. Pavone, E.A. Carter, Chem. Mater. **23**, 4525 (2011). https://doi.org/10.1021/cm201799c
32. G. Suchaneck, N. Kalanda, E. Artsiukh, G. Gerlach, Phys. Status Solidi B **257**, 1900312 (2020). https://doi.org/10.1002/pssb.201900312
33. M. Hoffmann, V.N. Antonov, L.V. Bekenov, K. Kokko, W. Hergert, A. Ernst, J. Phys.: Cond. Matt. **30**, 305801 (2018). https://doi.org/10.1088/1361-648x/aacb8d
34. N.A. Naushahi, I. Angervo, M. Saloaro, A. Schulman, H. Huhtinen, P. Paturi, J. Magn. Magn. Mater. **564**, 169990 (2022). https://doi.org/10.1016/j.jmmm.2022.169990
35. I. Angervo, M. Saloaro, J. Tikkanen, H. Huhtinen, P. Paturi, Appl. Surf. Sci. **396**, 754 (2017). https://doi.org/10.1016/j.apsusc.2016.11.021
36. M. Cernea, F. Vasiliu, C. Plapcianu, C. Bartha, I. Mercioniu, I. Pasuk, R. Lowndes, R. Trusca, G. Aldica, L. Pintilie, J. Eur. Ceram. Soc. **33**, 2483 (2013)
37. A. Dinia, J. Vénuat, S. Colis, G. Pourroy, Catal. Today **89**, 297 (2004)
38. L. Lutterotti, *Maud: Material Analysis Using Diffraction*, vol. 2.33 (http://maud.radiographema.com/, 1997). https://doi.org/10.1107/s1600576722006367/nb5328sup1.pdf
39. S. Nakamura, K. Oikawa, J. Phys. Soc. Jpn. **72**, 3123 (2003). https://doi.org/10.1143/jpsj.72.3123
40. S. Varaprasad, J. Mater. Sci: Mater Electron. **29**, 13606 (2018). https://doi.org/10.1007/s10854-018-9488-z
41. Y. Markandeya, K. Suresh, G. Bhikshamaiah, J. Alloys Compd. **509**, 9598 (2011). https://doi.org/10.1016/j.jallcom.2011.06.108
42. W. Jin-Feng, J. Am. Ceram. Soc. **97**, 1137 (2014). https://doi.org/10.1111/jace.12749
43. J. Blasco, C. Ritter, L. Morellon, P.A. Algarabel, J.M.D. Teresa, D. Serrate, J. Garcia, M.R. Ibarra, Solid State Sci. **4**, 651 (2002). https://doi.org/10.1016/s1293-2558(02)01309-2
44. C. Ritter, M.R. Ibarra, L. Morellon, J. Blasco, J. García, J.M.D. Teresa, J. Phys. Cond. Mat. **12**, 8295 (2000). https://doi.org/10.1088/0953-8984/12/38/306
45. B. García-Landa, C. Ritter, M.R. Iarra, J. Blasco, P.A. Algarbel, R. Mahendiran, J. García, Solid state commun. **110**, 435 (1999)
46. P. Paturi, M. Metsänoja, H. Huhtinen, Thin Solid Films **519**, 8047 (2011). https://doi.org/10.1016/j.tsf.2011.06.059
47. D. Yang, Phys. Rev. B **93**, 024101 (2016). https://doi.org/10.1016/j.jallcom.2017.09.027

48. J.L. Alonso, L.A. Fernández, F. Guinea, F. Lesmes, V. Martín-Mayor, Phys. Rev. B **67**, 214423 (2003). https://doi.org/10.1103/physrevb.67.214423
49. A. Misra, R.K. Thareja, J. Appl. Phys. **86**, 3438 (1999). https://doi.org/10.1063/1.371226
50. A.M. Reyes, Y. Arredondo, O. Navarro, J. Chem. Phys. **120**, 4048 (2016). https://doi.org/10.1007/s12648-017-0986-2
51. A.S. Ogale, S.B. Ogale, R. Ramesh, T. Venkatesan, Appl. Phys. Lett. **75**, 537 (1999). https://doi.org/10.1063/1.124440
52. W. Ji, J.F. Wang, J. Xu, L. Jiao, J. Zhou, Y.B. Chen, Z.B. Gu, S.H. Yao, S.T. Zhang, Y.F. Chen, J. Phys. D Appl. Phys. **46**, 015001 (2013). https://doi.org/10.1063/1.5024498
53. L. Balcells, J. Navarro, M. Bibes, A. Roig, B. Martinez, J. Foncuberta, Appl. Phys. Lett. **78**, 781 (2001). https://doi.org/10.1063/1.1346624
54. A.W. Sleight, J.F. Weiher, J. Phys. Chem. Solids **33**, 679 (1972). https://doi.org/10.1016/0022-3697(72)90076-5
55. T. Saha-Dasgupta, D.D. Sarma, Phys. Rev. B **64**, 064408 (2001). https://doi.org/10.1103/physrevb.64.064408
56. Y.H. Huang, M. Karppinen, H. Yamauchi, J.B. Goodenough, Phys. Rev. B **73**, 104408 (2006). https://doi.org/10.1103/physrevb.73.104408
57. G.Y. Liu, G.H. Rao, X.M. Feng, H.F. Yang, Z.W. Ouyang, W.F. Liu, J.K. Liang, J. Phys. Cond. Mat. **15**, 2053 (2003). https://doi.org/10.1016/s0925-8388(02)01316-6
58. B. Aguilar, O. Navarro, M. Avignon, Europhys. Lett. **88**, 67003 (2009). https://doi.org/10.1209/0295-5075/88/67003
59. Y. Hu, Y. Sun, X. Wang, J. Magnet. Magnet. Mater. **553**, 169234 (2022). https://doi.org/10.1016/j.jmmm.2022.169234
60. J. Lindén, T. Yamamoto, M. Karppinen, H. Yamauchi, T. Pietari, Appl. Phys. Lett. **76**, 2925 (2000). https://doi.org/10.1007/s12648-017-0986-2
61. J. Navarro, J. Fontcuberta, M. Izquierdo, J. Avila, M.C. Asensio, Phys. Rev. B **70**, 054423 (2004). https://doi.org/10.1103/physrevb.70.054423
62. B. Aguilar, O. Navarro, M. Avignon, Microelectron. J. **39**, 560 (2008). https://doi.org/10.1016/j.mejo.2007.07.034
63. J.H. Kim, S.C. Wi, S. Yoon, B.J. Suh, J.S. Kang, S.W. Han, K.H. Kim, A. Sekiyama, S. Kasai, S. Suga, C. Hwang, C.G. Olson, B.J. Park, B.W. Lee, J. Korean Phys. Soc. **43**, 416 (2003). https://doi.org/10.4283/jmag.2003.8.4.142
64. T.Y. Cai, Z.Y. Li, J. Phys. Cond. Mat. **16**, 3737 (2004). https://doi.org/10.1088/0953-8984/16/21/022
65. M. Hoffmann, A. Ernst, W. Hergert, V.N. Antonov, W.A. Adeagbo, R.M. Geilhufe, H. Ben Hamed, Phys. Status Solidi B **257**, 1900671 (2020)
66. J.P. Perdew, K. Burke, M. Ernzerhof, Phys. Rev. Lett. **77**, 3865 (1996)
67. V.I. Anisimov, J. Zaanen, O.K. Andersen, Phys. Rev. B **44**, 943 (1991)
68. A. Neroni, E. Sasioglu, H. Hadipour, C. Friedrich, S. Blugel, I. Mertig, M. Lezaic **100**, 115113 (2019). https://doi.org/10.1103/PhysRevB.100.115113
69. M. Hoffmann, V.N. Antonov, L.V. Bekenov, K. Kokko, W. Hergert, A. Ernst, J. Phys. Cond. Mat. **30**, 305801 (2018). https://doi.org/10.1088/1361-648x/aacb8d
70. B.L. Gyorffy, M.J. Stott, *Theory of Soft X-Ray Emission from Alloys* (Acad. Press, London and NY, 1973), pp.385–402
71. A. Liechtenstein, M. Katsnelson, V. Antropov, V. Ubanov, J. Magn. Magn. Mater. **67**, 65 (1987)
72. F. Ducastelle, F. Gautier, J. Phys. F: Metal Phys. **6**(11), 2039 (1976)